Overcoming the Torque/Stiffness Range Tradeoff in Antagonistic Variable Stiffness Actuators

Riccardo Mengacci, *Student Member, IEEE,* Manolo Garabini, *Member, IEEE,* Giorgio Grioli, *Member, IEEE,* Manuel G. Catalano, *Member, IEEE,* and Antonio Bicchi, *Fellow Member, IEEE,*

***Abstract*—To face the demand for applications in which robots have to safely interact with humans and the environment, the research community developed new types of actuators with compliant characteristics. To embody compliance into the actuator, elastic elements with fixed or variable compliance can be used. Among the variable stiffness mechanisms, a popular approach is based on the agonistic-antagonistic (A-A) layout, where two prime movers are elastically connected to the output shaft of the actuator. Notwithstanding the conceptually simple realization of the A-A layout, one limitation is that, due to the nonlinear torque/deflection characteristic of the elastic transmissions and to the limited spring elongation, the stiffness range achievable at the output shaft reduces as the external torque increases. In this work, a novel layout, based on the A-A principle, is proposed to increase the torque/stiffness capability of the actuator. To achieve this result, we combine elastic transmissions with linear and nonlinear torque/deflection characteristics. The mathematical model of the new layout and a possible implementation are analyzed. Then, the design of a novel variable stiffness actuator is presented and experimental validations are shown to compare the new device with the benchmark.**

***Index Terms*—Variable Stiffness Actuation, Antagonistic-VSAs, Soft Robotics, Modular Robots**

I. Introduction

Compliant robots are gaining more and more interest in the robotics community because of their capability to exhibit compliance in new scenarios where human beings and machines have to co-exist and co-operate [1]. In the last two decades, a novel generation of robots that embed compliant elements in their structures has been realized [2], inspired by the musculoskeletal structure of the vertebrate body [3].

The first compliant actuator proposed is composed of a prime mover (motor) connected to the output shaft through spring with constant elasticity. This is the so-called Series Elastic Actuator (SEA) introduced in [4]. Such actuators are employed in the realization of humanoid robots, such as WalkMan [5], iCub [6], and ESCHER [7] or quadrupedal robots such as Anymal [8]. Despite the easiest layout possible, in such systems, the stiffness is fixed and related to the spring physical properties. Conversely, the possibility of varying the torque/stiffness working point is implemented in Variable Stiffness Actuators (VSAs). Several prototypes of VSAs have been developed in the last years (for a detailed review see [2]). All these actuators require at least two motors in order to simultaneously and independently control the equilibrium position (or torque) and the stiffness of the output shaft. The latter may be obtained via two main different principles: by changing the transmission ratio between an elastic element and the output shaft, and by regulating the preload of elastic elements with nonlinear torque/deflection characteristics.

One of the prominent examples belonging to the first class is the AwAS, presented in [9], in which a linear spring is interposed between the prime mover and the output shaft. The position of the endpoint of the spring, and hence the stiffness of the output shaft, can be adjusted by the second motor. Other examples of actuators adopting a similar working principle are the CompAct-VSA prototype [10] and the vsaUT-II [11]. These actuators allow us to almost completely separate the actions of the motors (one mainly devoted to the control of output shaft position or torque and the other used for controlling the stiffness) and simplify the control design.

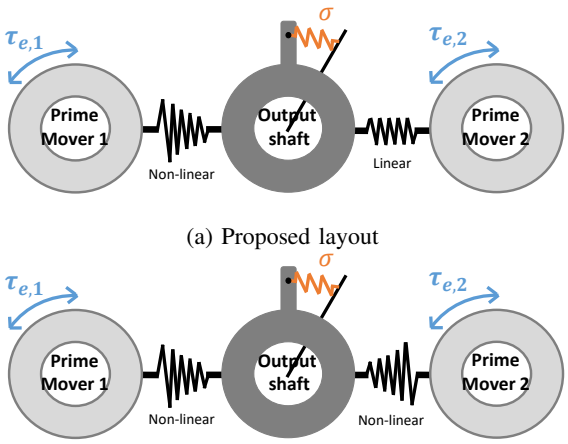

(a) Proposed layout

(b) Benchmark layout

Fig. 1: The conceptual scheme of the proposed A-A layout, Half Linear (HL), is shown in panel (a), while the original Fully Non Linear (FNL) layout, used here as benchmark, is depicted in panel (b). The main difference consists in the torque/deflection relations and the torque/stiffness profiles.

This work has received funding from the European Union's Horizon 2020 research and innovation program under agreement no. 780883 (THING), no. 871237 (SOPHIA), no. 101016970 (NI), no. 101017274 (DARKO), no. 871352 (ReconCycle) and from the Italian Ministry of Education and Research (MIUR) in the framework of the CrossLab project (Departments of Excellence). The content of this publication is the sole responsibility of the authors. The European Commission or its services cannot be held responsible for any use that may be made of the information it contains.

R. Mengacci, M. Garabini and A. Bicchi are with the Research Center "Enrico Piaggio", University of Pisa, Largo Lucio Lazzarino 1, 56126 Pisa, Italy (e-mail: *riccardo.mengacci/manolo.garabini/antonio.bicchi@gmail.com*)

G. Grioli, M. G. Catalano and A. Bicchi are with the Soft Robotics for Human Cooperation and Rehabilitation, Istituto Italiano di Tecnologia, via Morego, 30, 16163 Genova, Italy (e-mail: *giorgio.giroli/manuel.catalano@gmail.com*)

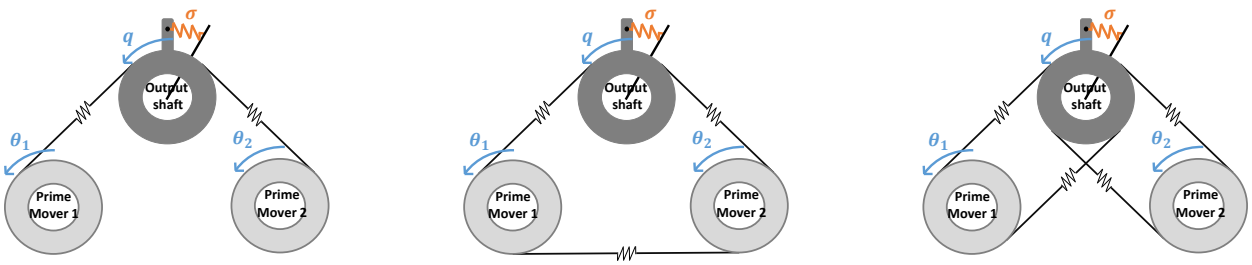

(a) Unirectional A-A (b) Cross-coupled A-A (c) Bidirectional A-A

Fig. 2: Variable stiffness mechanism based on different A-A layouts. Symbols refer to: θ_i angular position of i-th prime mover; q equilibirum position and σ stiffness of the output shaft.

However, the torque exhibited at the output link is limited to the torque provided by one motor.

Different layouts can be implemented to increase the actuator torque. One interesting example consists in the arrangement of the two prime-movers, together with the springs, in an agonist-antagonist (A-A) configuration. In the A-A layout, the motors can provide an output torque at the link up to the sum of the two motor torques when they operate in the so-called *helping mode* [12].

Although the conceptually simple implementation, one limitation in the use of A-A layouts concerns the restricted range of stiffness available at high external torques. This depends on the nonlinear torque/deflection characteristics and additionally to the bound on the elongation of the springs. Motivated by this, in this work we propose a different configuration, of such A-A layout, that allows enlarging the torque/stiffness range by combining spring mechanisms with linear and nonlinear torque/deflection characteristics (Fig. 1). Based on the proposed layout, the design and the realization of a new device, named *qbmove Advanced II*, is presented and compared to the previous prototype, the *qbmove Advanced I*, presented here as the benchmark. Besides the novel layout, the proposed actuator still presents the same benefits as the VSA-Cubes, thus it is modular, low cost, and has an intuitive and plug-and-play user interface (e.g. *Matlab/Simulink* [1] and *Robotic Operating System (ROS)* [2]). Furthermore, it is part of the open-source HW/SW tools made available by the *Natural Machine Motion Initiative (NMMI)*[3] [13], started by our group.

Sec. II presents the working principle of A-A actuators. Then, the limitation of the benchmark configuration is shown in Sec. III, while the proposed one is analyzed in Sec. IV. The physical A-A implementations and mathematical models are presented in Section V. Based on these models, the design and realization of the two prototypes are shown in Section VI. Preliminary experiments are shown in Sec. VII, while discussions and conclusions are drawn in Sec. VIII

II. Muscles for Compliant Robots

Among the possible designs of the elastic transmission of compliant actuators, (for a comprehensive review the reader may refer to [2]), the A-A layout is one of the most popular. The A-A layout is inspired by the arrangement of muscles that actuate the joints of vertebrate living beings. Indeed, in [3] it has been shown that a proper selection of the parameters of the elastic transmission (e.g. materials, geometry, etc.) can lead to torque/deflection characteristics very similar to the ones of biologic muscles. In the A-A layout, the possibility to vary the position and the compliance (stiffness) is allowed by two prime movers (motors) connected to an output shaft through elastic elements with nonlinear torque/deflection characteristics. In addition, both the motors can independently exert torque on the output shaft. Referring to Fig. 2 a rotation of both the prime movers in the same direction changes the equilibrium point of the output shaft, while a rotation in opposite directions results in a different working point for the elastic elements. Moving the motors in opposite directions changes the deflections of the elastic mechanisms, which corresponds, in the absence of external load, to a change in the stiffness since the torque/deflection characteristics are nonlinear. Three different arrangements for the elastic elements can be made: unidirectional (Fig. 2a), cross-coupled (Fig. 2b), or bidirectional (Fig. 2c). In the unidirectional layout, each motor can exert torque in only one direction. These actuators have the drawback that the maximum external torque that can be exerted at the output shaft corresponds to the maximum torque of a single motor, and no external torque can be generated in case of maximum stiffness. This layout is implemented e.g. in [14]. To tackle this problem in the cross-coupled layout a third elastic element is included to connect the two prime movers, resulting in the cross-coupled arrangements, as presented e.g. in [15]. A second layout that solves this problem is the bidirectional A-A (see Fig. 2c) in which each motor can exert torque in both directions on the output shaft. In both cross-coupled and bidirectional A-A actuators, the maximum torque at the output shaft is equal to the sum of the two motors. Two of the most relevant examples for the latter class of actuators are the BAVS actuator [12], used in the DLR Hand-Arm system [16], that is composed of two prime movers connected to the output shaft with an asymmetric cam disc variable stiffness mechanism, and the VSA-cube [17] in which the two prime movers are connected to the output shaft via a symmetric spring/tendon mechanism. A similar prototype based on springs/tendons has been presented in [18], while a different agonistic-antagonistic actuator based on compliant transmission elements (CTEs) has been investigated in [19].

[1] www.mathworks.com
[2] www.ros.org
[3] www.naturalmachinemotioninitiative.com

Focusing on the bidirectional A-A arrangement (Fig. 2c), in the following its torque/stiffness workspace is analyzed and a fundamental limitation, i.e. the decreasing of the stiffness range as the external torque increase, is presented.

III. Torque/Stiffness Range Limitation

According to [12], the torque τ that the elastic mechanisms, with the bidirectional A-A layout, can exert at the output shaft is given by

$$\tau_e(q, \theta_1, \theta_2) = \tau_{e,1}(\varphi_1) + \tau_{e,2}(\varphi_2), \tag{1}$$

where $\tau_{e,1}$ and $\tau_{e,2}$ represent the elastic torques of the mechanism that connect the output shaft to the motors, q is the position of the output shaft, θ_1 and θ_2 are the motor positions. Notice that the terms $\varphi_i = q - \theta_i,\ i = \{1, 2\}$ represent the deflection of each elastic mechanisms. Then, the stiffness of the output shaft $\sigma(q, \theta_1, \theta_2)$, i.e. its derivative w.r.t. the position q, is obtained as

$$\sigma(q, \theta_1, \theta_2) = \frac{\partial \tau(q, \theta_1, \theta_2)}{\partial q} = \underbrace{\frac{\partial \tau_{e,1}(\varphi_1)}{\partial q}}_{\sigma_1} + \underbrace{\frac{\partial \tau_{e,2}(\varphi_2)}{\partial q}}_{\sigma_2}. \tag{2}$$

Assuming that both the torque/deflection functions $\tau_{e,i}$ are invertible, it is possible to rewrite the output shaft stiffness (2) as function of the torque of the elastic mechanisms, i.e.

$$\sigma = \sigma_1(\tau_{e,1}) + \sigma_2(\tau_{e,2}). \tag{3}$$

In this way, given the following torque bounds of each motor-spring unit

$$|\tau_{e,1}| \leq \bar{\tau}, \quad |\tau_{e,2}| \leq \bar{\tau}\ , \tag{4}$$

where $\bar{\tau}$ is the maximum motor torque value; it is possible to evaluate for each external torque τ the maximum and minimum values of σ such that (1) and (3) are satisfied.

A common choice for the torque/deflection relation assumes an s-shaped two-terms exponential function [12], as follows

$$\tau_{e,i}(\varphi_i) = a_i \left(e^{b_i \varphi_i} - e^{-c_i \varphi_i}\right)\ , \tag{5}$$

where we assume the parameters $a_i, b_i, c_i = 1$ for the sake of simplicity. From (5) we can compute the following stiffness

$$\sigma_i(\varphi_i) = b_i \tau_{e,i}(\varphi_i) + a_i(b_i + c_i)e^{-c_i \varphi_i}\ , \tag{6}$$

that is linear w.r.t. the elastic torque and has a stress-stiffening behavior. This behavior, differently from the stress-softening one, implies that an increment of the position displacement acts to increase the elastic torque that, in turn, increases the stiffness of the elastic element. Throughout this paper, we will focus on this behavior that found many examples in practical applications (see e.g., [2]).

Furthermore, we assume that the two elastic characteristics are equal, thus that the elastic elements have the same properties, i.e. the mechanism is symmetric. This implies e.g., that the springs are subjected to the same constraints on the elongations. From now on, we will refer to this benchmark layout with the term *Fully Non Linear (FNL)* configuration (Fig. 1b).

For bidirectional A-A presenting both the motor-spring units with a nonlinear torque/deflection characteristic as in (5), the torque/stiffness workspace is shown in Fig. 3. More in detail, Fig. 3a shows the link stiffness w.r.t the motor-spring torques $\tau_{e,i}$, while in Fig. 3b the relationship between the link stiffness and the sum of the two unit torques is reported. It is worth recalling that the summation of the two unit torques is equal to the torque at the output shaft (see (1)) and reflects also the external torque. Furthermore, it is limited to twice the maximum torque $\bar{\tau}$ of each motor.

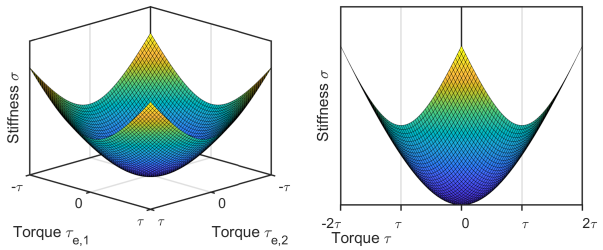

(a) (b)

Fig. 3: Torque/stiffness workspaces for the FNL configuration shown in Fig. 1. In (a) the two separate motor-spring unit torques are reported w.r.t. the output shaft stiffness, while in (b) the summation of the two torques vs. the stiffness is shown.

For the FNL configuration case, the analysis of the torque/stiffness workspace leads to the following considerations: 1) the admissible range of stiffness reduces as the output torque increases; 2) the full range of stiffness (in particular the minimum value) can be achieved only at zero external torque. Note that, the first point is a direct consequence of the stress-stiffening nature of the torque/deflection characteristics of the elastic mechanisms that we consider in this paper.

The two limitations listed above can also be seen in Fig. 3. More specifically, referring to Fig. 3b, we can conclude that, if the two motor-spring units work opposite of the same amount then, under the symmetry assumption, the output torque τ is zero. Consequently, the stiffness value can be set to the minimum or to the maximum value. This is the ideal working condition of a bidirectional A-A layout. Differently, as soon as the external torque increases, the available stiffness range decreases, up to the point to reach zero if the two motors reach the maximum torque ($\pm 2\tau$ in Fig. 3b). This is the point in which the two motors enter the helping mode, i.e. they both sustain the external load without the possibility of changing the stiffness. Furthermore, it is important to say that the minimum and maximum stiffness values reached are strictly dependent on the mechanical characteristics of the actuator, e.g. motor torques and spring/tendon properties. In this section, we analyzed such workspace from a theoretical point of view, while the results for the real implementations will be discussed in Section VII.

IV. Proposed Half-Linear Configuration

To overcome the limitations stated in the previous section, the configuration proposed in this work replaces one side of the bidirectional layout with an elastic mechanism with a linear torque/deflection characteristic. To the best of our knowledge, in literature, there are no examples of A-A VSA exploiting this

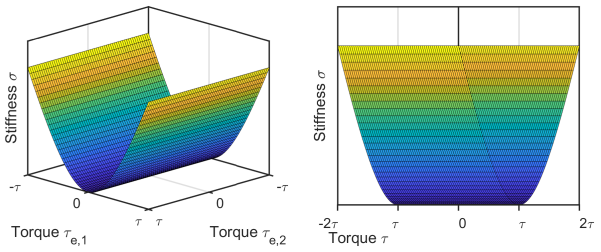

(a) (b)

Fig. 4: Torque/stiffness workspaces for the HL configuration shown in Fig. 1. In (a) the two separate motor-spring unit torques are reported w.r.t. the output shaft stiffness, while in (b) the summation of the two torques vs. the stiffness is shown.

combination. One attempt to combine two different branches of A-A actuators has been presented in [20]. However, the case of a series elastic actuator (SEA) in conjunction with a parallel elastic (PE) element for energy storage is considered. Thus, the stiffness values of the two different branches must be designed offline.

From now on we will refer to the proposed layout with the term *Half Linear (HL)* configuration (Fig. 1a). The motor-spring unit torque is given as follows

$$\begin{cases} \tau_{e,i}(\varphi_i) = a_i \left(e^{b_i \varphi_i} - e^{-c_i \varphi_i} \right), & i \text{ nonlinear}, \\ \tau_{e,i}(\varphi_i) = k_i(\varphi_i - d_i), & i \text{ linear}, \end{cases} \tag{7}$$

and the resulting stiffness is

$$\begin{cases} \sigma_i(\varphi_i) = b_i \tau_{e,i}(\varphi_i) + a_i(b_i + c_i) e^{-c_i \varphi_i}, i \text{ nonlinear}, \\ \sigma_i = k_i, \qquad\qquad\qquad\qquad\qquad\quad i \text{ linear}, \end{cases} \tag{8}$$

assuming for simplicity $a_i, b_i, c_i = 1$ and also $k_i = 1, d_i = 0$.

The torque/stiffness workspace of the HL layout is shown in Fig. 4. By analyzing the torque/stiffness characteristics reported in this figure, it is possible to see the two benefits of the proposed configuration. The first one is that, if high output link torques are requested (close to $\pm 2\tau$ in the plots), the new layout allows a larger stiffness range compared to the FNL case. On the other side, the HL configuration allows maintaining low stiffness value for an higher external torque. This can be seen from the plots in Fig. 4b and Fig. 3b by comparing the minimum value of the stiffness of the two layouts at the particular external torque τ. Note that, even in this case, the values reached by these plots are strictly dependent on the mechanical characteristics of the actuator, and real considerations will be debated in Section VII. The presence of these two features can be particularly useful in real applications where external collisions may occur at high torques. Indeed, at high torques correspond high risk of damages for the mechanical parts. Furthermore, by inserting the linear motor-spring unit, the capability of the actuator to exploit a compliant behavior while working in presence of gravity is increased. Indeed, the stiffness of the linear motor-spring unit can be properly designed to meet the load requirements of the task to be accomplished, without affecting the stiffness variation range.

V. Bidirectional A-A Implementations

In this section, we present one of the possible strategies to implement the proposed bidirectional A-A configurations as well as the benchmark. The chosen strategy is based on the spring/tendon scheme, as visible in Fig. 5.

For what concerns the benchmark case (FNL), two elastic elements (linear extension springs) connect the two prime movers to the output link through a pair of tendons (yellow and red lines in Fig. 5b). Instead, to implement the proposed HL configuration the scheme in Fig. 5a is investigated, in which one of the nonlinear units is replaced with one unit with linear torque/deflection relation. For both the configurations, due to the presence of, at least one, nonlinear motor-spring unit, the torque/deflection seen at the output shaft results nonlinear (Section VII). According to [21], this condition ensures the possibility of varying the stiffness. Indeed, in this way the stiffness computation becomes dependent on the motor deflections, thus can be properly varied, differently from what happens in the linear case, in which the stiffness is constant (cf. first and second equation in (8)).

In the following, the mathematical models of such configurations are analytically analyzed and simplified models, based on the torque/deflection and torque/stiffness characteristics shown in the previous sections, are presented.

A. Linear and Nonlinear Characteristics

As introduced previously, the proposed HL configuration consists of one nonlinear (Fig. 6a) and one linear unit (Fig. 7a), while the FNL configuration is realized with two nonlinear elastic units (Fig. 6a). In the following, the model of both these nonlinear and linear units is presented. Furthermore, due to the symmetry of such units, only one branch (the upper) will be mathematically modeled. This branch is shown in Fig. 6b for the nonlinear case, while is depicted in Fig. 7b for the linear case. The summation of two branches gives then the overall torque/deflection relation of the single units. To compute the analytic model of the units, we assume the following:

S.1: Each tendon, that connects the prime movers to the output shaft, has a fixed length, i.e. it can not elongate through time.

Nonlinear unit model: The useful dimensions of the branch for the nonlinear unit are depicted in Fig. 6b. Starting from assumption *S.1*, the following constraint on the length of the tendon holds

$$L_1 + L_2 + L_\theta + L_\mathrm{q} = L_\mathrm{T} \ , \tag{9}$$

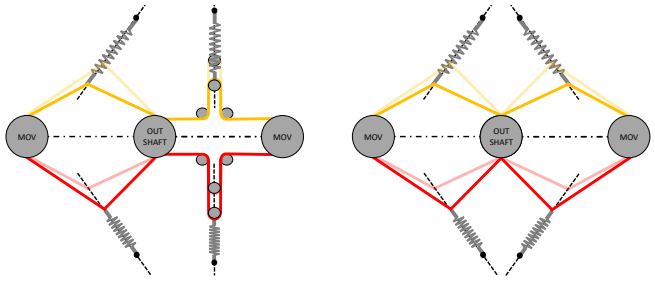

(a) HL (b) FNL

Fig. 5: Spring/tendon implementation of the two layouts.

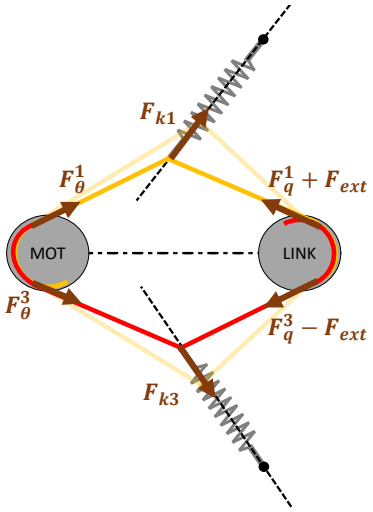

(a) Forces scheme for the non linear unit of the stiffness mechanism. Symbols of the figure represent: $F_{kj}, F_\theta^j, F_\mathrm{q}^j$ force of spring j-th, motor and link force component of j-th branch, for $j = 1, 3$, respectively, and F_ext the external force.

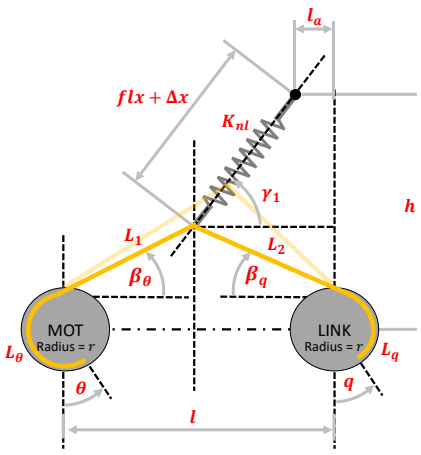

(b) Branch n.1 (upper) of the non linear stiffness mechanism in elongation case. Symbols in the figure represent: θ, q angular positions of motor and link, respectively; l distance between the driving pulley and output link; h, l_a anchor points of the spring; γ_1 anchor angle of the spring movement; $flx, \Delta x$ free length, and elongation of the spring and K_nl spring constant.

Fig. 6: Schemes of the overall unit (a) and the upper branch (b) for the nonlinear case.

where L_1, L_2 are the portions of tendon at the left and right side of the spring after an angular displacement of the motors (or the link), as shown in Fig. 6b, L_θ is the portion of tendon wrapped around the driving pulley, L_q is the portion of tendon wrapped around the output link pulley (not actuated) and L_T is the total length of the tendon (supposed constant *S.1*).

To describe how the spring elongates (i.e. find Δx) when the output shaft (or the driving pulley) rotates, it is necessary to solve the following system of equations

$$\begin{cases} r\cos(\beta_\theta) + L_1\sin(\beta_\theta) + (flx + \Delta x)\sin(\gamma_1) = h \\ r\cos(\beta_\mathrm{q}) + L_2\sin(\beta_\mathrm{q}) + (flx + \Delta x)\sin(\gamma_1) = h \\ l_a + (flx + \Delta x)\cos(\gamma_1) + L_1\cos(\beta_\theta) - r\sin(\beta_\theta) = l \\ L_1 + L_2 + r(2\pi \mp (q - \theta_i) - \beta_\mathrm{q} - \beta_\theta) = L_\mathrm{T} \end{cases} , \tag{10}$$

where $\beta_\theta = \beta_\theta(q, \theta_i)$ and $\beta_\mathrm{q} = \beta_\mathrm{q}(q, \theta_i)$ are the angles shown in Fig. 6b, different between motor and output shaft pulleys. The motor position θ_i represents the position of the i-th prime mover and the terms h, l, l_a, r, γ_1 are constructive parameters. The sign of the term $(q - \theta_i)$ in the last equation of (10) depends on the branch considered (upper $(-)$, lower $(+)$). It is worth noting that the solution (Δx) of (10) can not be found in an explicit form for the mechanism geometry.

In Fig. 6a the overall forces acting on the nonlinear unit are reported. From this force representation it is possible to compute the total force applied at the link by this unit as

$$\begin{cases} F_\mathrm{q}^1 = -\frac{\frac{\tau_{\theta_i}}{r}(\cos(\beta_\theta^1)+\sin(\beta_\theta^1)) + K_\mathrm{nl}\Delta x^1(\cos(\gamma_1^1)+\sin(\gamma_1^1))}{(\cos(\beta_\mathrm{q}^1)+\sin(\beta_\mathrm{q}^1))} - \frac{\tau_\mathrm{ext}}{2r} \\ F_\mathrm{q}^3 = -\frac{\frac{\tau_{\theta_i}}{r}(\cos(\beta_\theta^3)+\sin(\beta_\theta^3)) + K_\mathrm{nl}\Delta x^3(\cos(\gamma_1^3)+\sin(\gamma_1^3))}{(\cos(\beta_\mathrm{q}^3)+\sin(\beta_\mathrm{q}^3))} + \frac{\tau_\mathrm{ext}}{2r} \end{cases} , \tag{11}$$

where F_q^1 is the force component exhibited on the link from the upper branch, while F_q^3 is the force component exhibited on the link from the lower branch (see Fig. 6a). The term K_nl is the spring constant (supposed indentical for both the branches), $\tau_{\theta_i} = rF_\theta$ is the i-th motor torque (after the gear-box) and $\tau_\mathrm{ext} = rF_\mathrm{ext}$ is the external torque. From (11) the torque component of the i-th nonlinear unit is computed as $\tau_{\mathrm{u},i}^\mathrm{nl} = r(F_\mathrm{q}^3 - F_\mathrm{q}^1)$. Since our interest is to find the elastic torque exerted at the link related to an angular displacement, it is possible to extrapolate from (11) only the following elastic contributes

$$\begin{cases} F_{k1} = -K_\mathrm{nl}\Delta x^1 \frac{(\cos(\gamma_1^1)+\sin(\gamma_1^1))}{(\cos(\beta_\mathrm{q}^1)+\sin(\beta_\mathrm{q}^1))} \\ F_{k3} = -K_\mathrm{nl}\Delta x^3 \frac{(\cos(\gamma_1^3)+\sin(\gamma_1^3))}{(\cos(\beta_\mathrm{q}^3)+\sin(\beta_\mathrm{q}^3))} \end{cases} , \tag{12}$$

and the total elastic torque contribution of the i-th unit at the output shaft becomes

$$\tau_{\mathrm{e},i}^\mathrm{nl} = r(F_{k3} - F_{k1}) \ . \tag{13}$$

Due to the presence of the spring elongation terms $\Delta x^{1,3}$, the relation (13) depends on both motor and output shaft angular position. However, it can not be expressed w.r.t. their difference, i.e. the deflection $\varphi_i = q - \theta_i$. Thus, the desired torque/deflection model must be identified following the identification method presented in [22]. The identification is based on angular measurements and torques data collected from cyclic tasks executed on the real prototype.

According to what stated in Section II, to find a fitting curve from the experimental data the following model is adopted

$$\tau_{\mathrm{e},i}^\mathrm{nl} = a_i\left(e^{b_i\varphi_i} - e^{-c_i\varphi_i}\right) \ , \tag{14}$$

where $a_i, b_i, c_i > 0$.

Linear unit model: Even in the linear case, only one branch can be analyzed (shown in Fig. 7b) since the linear unit is symmetric as visible in Fig. 7a. The useful dimensions of this branch can be retrieved from Fig. 7b.

For this simplified case, to describe how the spring elongates (i.e. find Δx) after an angular displacement between the motor

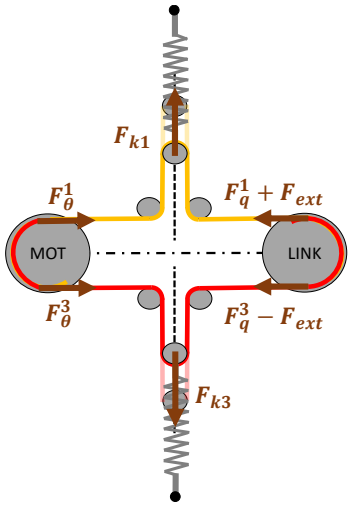

(a) Forces scheme for the linear unit of the siffness mechanism. Symbols of the figure represent: $F_{kj}, F_\theta^j, F_q^j$ force of spring j-th, motor and link force component of j-th branch for $j = 1, 3$, respectively, and F_{ext} the external force.

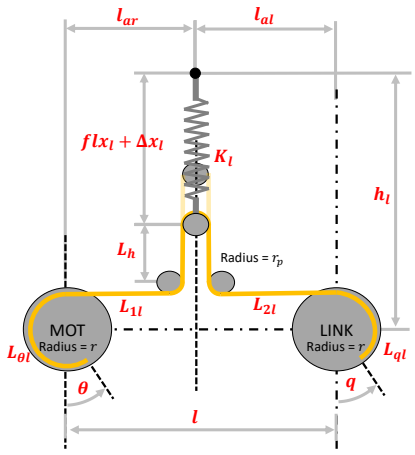

(b) Branch n.1 (upper) of the linear stiffness mechanism in elongation case. Symbols in figure represent: θ, q angular positions of motor and link, respectively; l distance between driving pulley and output link; h_l anchor point of the spring; $flx_l, \Delta x_l$ free length and elongation of the spring and K_l spring constant. Note that in this particular case L_{1l} and L_{2l} are fixed and $L_{ql} + L_{\theta l} = r(2\pi \mp (q - \theta))$.

Fig. 7: Schemes of the overall unit (a) and the upper branch (b) for the linear case.

pulley and the output shaft, the following system of equations (15) have to be solved

$$\begin{cases} r + r_p + L_h + flx_l + \Delta x_l = h_l \\ L_{1l} + L_{2l} + r(2\pi \mp (q - \theta_i)) + 2\pi r_p + 2L_h = L_{\text{T}} \end{cases} , \tag{15}$$

where the terms h_l, r, r_p are constructive parameters and we assume the validity of *S.1*. All the other symbols are described in Fig. 7b. Note that, even for this computation, the sign of the term $(q - \theta_i)$ in the last equation of (15) depends on the branch considered (upper $(-)$, lower $(+)$).

Differently, from the case in (10), the spring elongation can be computed, starting from the angular displacement, as

$$\Delta x_l = h_l - flx_l - r - r_p - \frac{(L_{\text{T}} - l_{al} - l_{ar})}{2} + \pi(r + \frac{r_p}{2}) \mp \frac{r(q - \theta_i)}{2}.$$

Then, from the forces representation reported in Fig. 7a it is possible to compute the total torque applied at the link by the i-th unit as $\tau_{\text{u},i}^{\text{l}} = r(F_{q3} - F_{q1}) = -r^2 K_{\text{l}}(q - \theta_i) + \tau_{\text{ext}}$, where

$$\begin{cases} F_{q1} = -\left(K_{\text{l}}\Delta x^1 + \dfrac{\tau_{\theta_i}}{r} + \dfrac{\tau_{\text{ext}}}{2r}\right) \\ F_{q3} = -\left(K_{\text{l}}\Delta x^3 + \dfrac{\tau_{\theta_i}}{r} - \dfrac{\tau_{\text{ext}}}{2r}\right) \end{cases} . \tag{16}$$

Considering only the elastic components as before gives

$$\begin{cases} F_{k1} = -K_{\text{l}}\Delta x^1 \\ F_{k3} = -K_{\text{l}}\Delta x^3 \end{cases} , \tag{17}$$

and the total elastic torque at the output link of the i-th linear unit becomes

$$\tau_{\text{e},i}^{\text{l}} = r(F_{k3} - F_{k1}) = -r^2 K_{\text{l}}(q - \theta_i) \ . \tag{18}$$

It is worth noting that, differently from the nonlinear case, (18) describes analytically the torque/deflection relation. However, despite the equation (18) can be directly evaluated, to take into account variability of mechanical parameters and wear phenomena it is possible to identify the elastic constant from experimental data with the function presented in Section IV, i.e.,

$$\tau_{\text{e},i}^{\text{l}} = k_i(\varphi_i - d_i) \ , \tag{19}$$

where now $k_i, d_i > 0$ and d_i represents a possible bias on the angular displacement due to mechanical irregularities.

To evaluate the compliant behavior of the actuator, starting from the identified torque models in (14) and in (19), the stiffness of each unit (σ_i^{nl} and σ_i^{l}) are computed using (6) and (8), respectively.

Finally, combining the units described in this section (nonlinear and linear), it is possible to build the two different configurations for the variable stiffness mechanism, as stated previously: the proposed half linear (HL) (Fig. 5a) and the benchmark fully nonlinear (FNL) (Fig. 5b), modeled as

$$\begin{cases} \tau_e^{\text{HL}} = \tau_{\text{e},1}^{\text{nl}} + \tau_{\text{e},2}^{\text{l}} \\ \sigma^{\text{HL}} = \sigma_1^{\text{nl}} + \sigma_2^{\text{l}} \end{cases} , \quad \begin{cases} \tau_e^{\text{FNL}} = \tau_{\text{e},1}^{\text{nl}} + \tau_{\text{e},2}^{\text{nl}} \\ \sigma^{\text{FNL}} = \sigma_1^{\text{nl}} + \sigma_2^{\text{nl}} \end{cases} . \tag{20}$$

VI. Actuators Design and Realization

Based on the proposed HL configuration analyzed in the previous sections, in the following, the design and the mechanical/electrical realization of a novel VSA prototype, namely *qbmove Advanced II*, is described. Furthermore, we present the realization of the *qbmove Advanced I* prototype, an improvement of the VSA-Cube concept [17] that implements the original idea of the FNL configuration. The latter is used here for comparison as a benchmark. Since the two differ only for the variable stiffness mechanism then, except for Section VI-2, the description of mechanical (VI-1) and electrical (VI-3) parts of the actuator are valid for both the prototypes. These prototypes preserve the benefits of modularity, open-source,

and easy-to-use interface and are part of the NMMI [13] started by our research group.

The overall shape of the qbmove Advanced I and II VSA is a cube with 66 mm edges as depicted in Fig. 8a. As for the VSA-Cube concept, the frame presents small grooves along the edges used to interconnect the single actuator with other modules [13]. To reduce the weight of the actuator, without compromise its strength, the frame is realized with injection molding technology. The main features are summarized in the table in Fig. 8a. The device is composed by three principal parts (Fig. 8b): top frame (**i**), main frame (**ii**), and bottom frame (**iii**). The top frame is used to cover the variable stiffness mechanism and to hold the output shaft through a roll bearing, while the other two frames contain the mechanics and the custom electronics.

1) Mechanical frame: This frame represents the core of both the actuator prototypes. Indeed, it is composed of two motor units made up of two conventional dc motors (prime movers)(**1**), and two customized serial gear-boxes (**2**). The motors, model *DCX22S-GB-SL-24V* manufactured by Maxon Motor company, are powered by a 24 V supply voltage and can exert a continuous torque of $\tau_m = 14.9\,\text{Nmm}$, with 22.6 W of nominal power. In series, there is a custom gear-box with five reduction stages. The reduction ratio of each gear-box

	FNL	HL
Power supply	24 V	
Nominal torque	$\tau \simeq 6.1$ Nm	
Nominal speed	$v_p \simeq 5.5$ rad/s	
Active rotation angle	±3.14 rad	
Passive Deflection (approx.)	[0.20 − 0.61] rad [max. − min.] stiffness	
Stiffness Range (approx.)	[0.01 − 70] Nm/rad	[0.35 − 35] Nm/rad
Max. Elastic Energy (approx.)	0.66 J	0.80 J
Encoder (x3)	12 bit	
Dimensions	66x66x66 mm	
Weight	0.45 kg	

(a) Real prototype with main features.

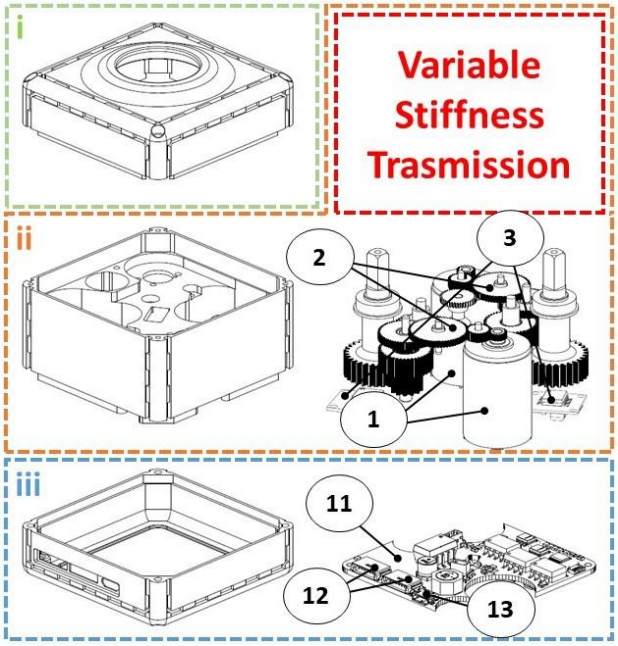

(b) Exploded view. Top frame (**i**), main frame (**ii**), and bottom frame (**iii**) with their main inner components. The two stiffness mechanisms are instead detailed in Fig. 9a and Fig. 9b.

Fig. 8: qbmove Advanced design.

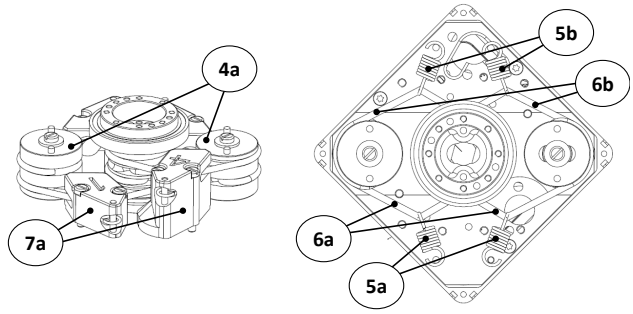

(a) FNL configuration

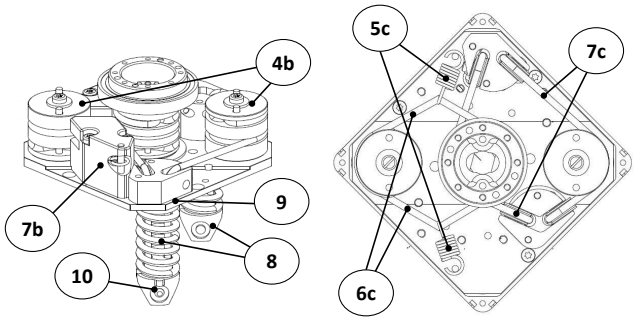

(b) HL configuration

Fig. 9: Detailed views of the variable stiffness mechanism realized for the qbmove Advanced I (a) and the qbmove Advanced II (b). Lateral (left-hand side) and top (right-hand side) views are reported in panel (a) and (b).

system is $1:205$ and allows to provide at the output of each gear-box a torque of $\tau_p \simeq 3.05\,\text{Nm}$ and a maximum speed of $v_p \simeq 5.5\,\text{rad/s}$. Since the two motor units can work in parallel, the final output torque of the actuator is about $\tau \simeq 6.1\,\text{Nm}$ (in continuous mode and neglecting the gear-box efficiency). Finally, the two prime mover pulleys and the output link have a magnetic encoder (**3**) in order to measure the angular positions. The encoders are the ones produced by Austria Microsystem, *AS5045* type, with 12-bit resolution.

2) Variable Stiffness Transmission: According to the models shown in Section V, the variable stiffness mechanism can be realized in two different layouts: one with two non linear units (FNL, Fig. 5b), and another one with one unit replaced with a linear subsystem (HL, Fig. 5a). Both configurations implement the bidirectional A-A principle. This implies that when the two pulleys rotate in opposite directions, the springs are loaded and their working point change resulting in a different stiffness behavior. Differently, when the pulleys rotate in the same directions, the output shaft moves. Referring to Fig. 9a and Fig. 9b, two machined aluminum pulleys are connected at the end of the gear-boxes (**4a**, **4b**). The design of the spring/tendon mechanism for the FNL configuration is depicted in Fig. 9a. It is realized with four linear extension springs[4] (**5a**, **5b**) and four *Dyneema* tendons (**6a**, **6b**), model *DC-200-CARBON-GREY-LIROS*. One side of the springs is fixed and their movements are constrained inside a plastic guide (**7a**), while the tendons are connected to both the output

[4]Product code: U.045.065.0127.IX (https://www.vanel.com/)

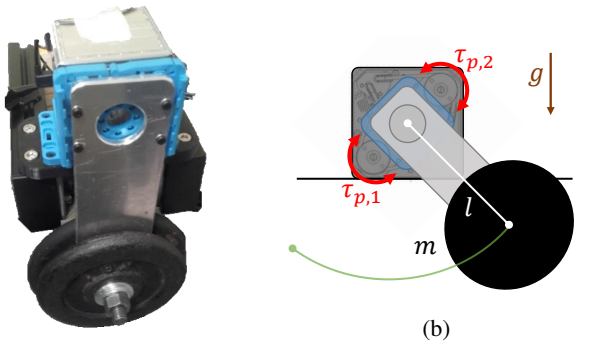

(a) (b)

Fig. 10: Experimental setup (a) and sketch (b). The two prime movers are controlled in position, through a low-level PD controller, for the quasi-static identification, while they are controlled in torque for the stiffness evaluation test.

shaft and the pulley via pins. For what concern the design of the HL configuration, shown in Fig. 9b, the left side, as for the FNL case, presents two extension springs (**5c**), that move inside plastic guides (**7b**), and two tendons (**6c**). The right side instead, is realized with two compression springs[5] (**8**). Different from the extension springs, these types of springs allow to increase the torque/deflection capability of the motor-spring unit and to reduce the loss of performances due to springs loosening phenomena. One side of each spring is fixed at the frame (**9**), while the other side is connected to an idler pulley (**10**). Two similar *Dyneema* tendons connect the motor pulleys at the output shaft (**7c**).

3) Electronic frame: The entire electronic control board is placed inside this third frame. In this way all the connections with the main frame components are easy to access and the device maintains a compact structure. The board is a custom PCB (**11**) provided with a *Cypress PSoC 3* micro-controller, two h-bridges to drive the motors, two current sensors, and a voltage sensor. Several control policies are implemented inside the open-source custom firmware (FW) (download available on the NMMI website). The prime movers can be controlled either in position mode, leading to a *servo-control* system, or in currents. However, the open-source philosophy allows the user to develop and to implement more complex low-level strategies, without limitations. As an example, more sophisticated control police, already implemented on-board, allows regulating simultaneously the output shaft position and the stiffness of the device through semi-sum and semi-difference of prime movers positions, as discussed in [15]. To power both logic and motors a pair of mini bridge connectors[6], produced by *ERNI Electronics* company, are placed (**12**). Through these connectors, it is also possible to interconnect multiple NMMI modules, each one with its own identifier, in a *daisy-chain* topology. Instead, a micro-USB (**13**) connector allows to upload the control firmware and to communicate with the user interfaces, e.g. *Matlab/Simulink* [23] or *Robotic Operating System (ROS)* (www.ros.org). The communication protocol for each device is the serial *RS485*.

[5]Product code: C.140.220.0250.AP (https://www.vanel.com/)
[6]Datasheet: https://docs.rs-online.com/332d/A700000006973564.pdf

VII. Experimental Tests

The experimental tests in the following analyze and compare the models presented in Section V with the real characteristics of the prototypes built in Section VI. First, a quasi-static identification is performed to retrieve the model parameters of the layout of the two prototypes, i.e. qbmove Advanced I and qbmove Advanced II. Then, from the identified models the stiffness is evaluated and compared among the two prototypes.

From (20) it is possible to obtain the torque/deflection and stiffness of both the configurations. More in details, for the proposed HL layout composed by one linear unit the model is given by

$$\begin{cases} \tau_e^{\text{HL}} = a_1 \left(e^{b_1\varphi_1} - e^{-c_1\varphi_1}\right) + k_2(\varphi_2 - d_2) \\ \sigma^{\text{HL}} = a_1 \left(b_1 e^{b_1\varphi_1} + c_1 e^{-c_1\varphi_1}\right) + k_2 \end{cases} . \tag{21}$$

Instead, for the benchmark one (FNL) the equations are

$$\begin{cases} \tau_e^{\text{FNL}} = a_1 \left(e^{b_1\varphi_1} - e^{-c_1\varphi_1}\right) + a_2 \left(e^{b_2\varphi_2} - e^{-c_2\varphi_2}\right) \\ \sigma^{\text{FNL}} = a_1 \left(b_1 e^{b_1\varphi_1} + c_1 e^{-c_1\varphi_1}\right) + a_2 \left(b_2 e^{b_2\varphi_2} + c_2 e^{-c_2\varphi_2}\right) \end{cases} . \tag{22}$$

A. Quasi-static identifications

Through quasi-static tests, we identified the torque/deflection model parameters of each unit of both prototypes. The experimental steps, described in [22], consist of load-unload cycles at the output shaft of the actuators using a rigid bar equipped with a mass at the end (Fig. 10). The mass weight used in the test is $m = 2\,\text{kg}$ and the center of mass, of the link/weight structure, is at $l = 0.16\,\text{m}$ from the center of rotation. This corresponds to an external torque of $3.14\,\text{Nm}$ at $1.57\,\text{rad}$ (recall that the nominal torque exploited by each motor unit is about $3.05\,\text{Nm}$). We decide to not exceed this value to protect the structure from mechanical damages. To avoid coupling effect between the two motor-spring units, the two units are identified separately, then the whole mechanism is tested. This means that, while the prime mover of one unit is position-controlled to the desired reference, the position of the other one is such that it tracks the link angle. The reference position for each unit was a sinusoidal wave with a frequency of $[0.08\ 0.06\ 0.04\ 0.02]\,\text{Hz}$ and a fixed amplitude of $1.74\,\text{rad}$.

Results: The results for the identification of the two motor units of the qbmove Advanced I prototype with the FNL configuration are depicted in Fig. 11a and Fig. 11b where the fitting models (solid red lines) are compared with the experimental data (cyan points). Similarly, the results for both

unit i	$a_i[\text{Nm}]$	$b_i[\text{rad}^{-1}]$	$c_i[\text{rad}^{-1}]$
1	$2.097e^{-4}$	11.77	8.862
2	$1.005e^{-4}$	14.6	9.248

TABLE I: Fully Non Linear (FNL) model parameters

unit i	$a_i[\text{Nm}]$	$b_i[\text{rad}^{-1}]$	$c_i[\text{rad}^{-1}]$	$k_i[\frac{\text{Nm}}{\text{rad}}]$	$d_i[\text{rad}]$
1	$6.503e^{-5}$	11.29	10.63	–	–
2	–	–	–	0.3546	0.3055

TABLE II: Half Linear (HL) model parameters

the nonlinear and linear units of the qbmove Advanced II prototype with the HL configuration are reported in Fig. 11c and Fig. 11d. The cyan points are the experimental data while the red solid lines are the fitting curves. Figures 12a and 12b report the torque/deflection characteristic at the link obtained by further experimental trials where the prototypes are controlled through equilibrium reference, semi-sum of motor positions, and stiffness preset, semi-difference of motor positions [13]. The five stiffnesses tested are obtained by imposing a fixed pretensioning of $\theta_{sr} = [0,\ 0.125,\ 0.25,\ 0.375,\ 0.5]$ rad. The overall identified parameters for the FNL stiffness mechanism are also summarized in Table I, while in Table II the ones for the HL stiffness mechanism are reported.

The first consideration for these results is relative to the fact that the curves are affected by hysteresis cycles, more noticeable for the HL configuration case. This behavior is unavoidable if frictional effects, combined with elastic elements, affect the system, but does not represent a limitation for the analysis proposed in this work. Furthermore, even if the variable stiffness mechanisms of the nonlinear units are supposed to be identical, i.e. equal tendon lengths and springs (cf. Section VI-2), there are considerable differences between the units of the two prototypes. More in detail, the maximum deflections are different for positive or negative directions and dependent on the unit considered. This is mostly due to relaxing phenomena of the springs and the elongation shown by the tendons [24], and leads to asymmetric branches.

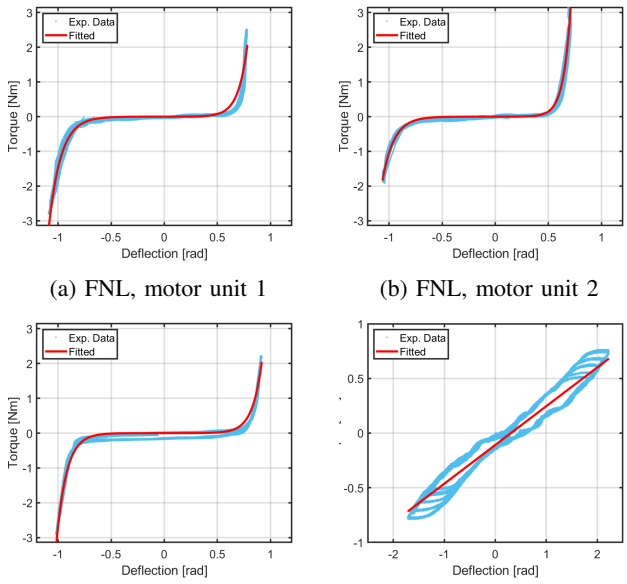

(a) FNL, motor unit 1 (b) FNL, motor unit 2

(c) HL, motor unit 1 (d) HL, motor unit 2

Fig. 11: Experimental data (cyan points) and identified torque/deflection characteristics (solid red lines) of each motor unit of the two configurations, i.e. FNL and HL. Note that, despite the mechanisms of the nonlinear units are the same, due to the fact that assumption *S.1* is not verified and friction effects, there are notably differences in the curves. The models fitting parameters are summarized in Table I and Table II.

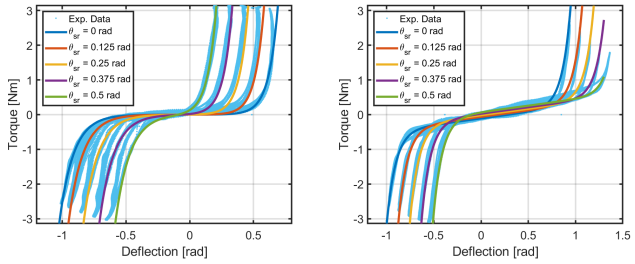

(a) FNL, link (b) HL, link

Fig. 12: Experimental data (cyan points) of the torque/deflection at the link together with the curves obtained evaluating the identified functions (solid colored lines) for five different stiffnesses, imposed by θ_{sr}.

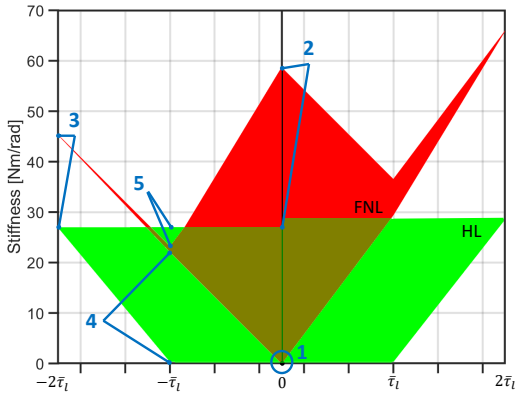

Fig. 13: Torque/stiffness workspaces for the two prototype configurations, FNL in red and HL in green. The points highlighted represent: **1**) zero external load; **2**) zero external load and pretension of the motors; **3**) both motors loaded to sustain an external load; **4**) external torque held by the two motors, for the FNL case, and from the linear part only, for the HL case; **5**) only the (one in the FNL case) nonlinear unit holds the external load.

B. *Stiffness evaluation*

To evaluate the stiffness of the two prototypes we perform an experiment similar to the previous one, in which the motors are now torque-controlled. Using the same setup in Fig. 10, differently from other evaluation methods, e.g, the ones based on ball-impacts [18], it is possible to exactly imposing the desired torque at each motor unit and to limit it to the maximum load torque, i.e. $\tau_{p,i} < \tau_l = \pm 3\,\text{Nm}$, by controlling[7] the swing angle of the output shaft (green line in Fig. 10). To the sake of clarity, without loss of generality, we report the stiffness evaluation only for negative external torques, i.e., positive motor torques. The case of positive external torques can be evaluated similarly by exploiting, however, the slightly different range of stiffness due to the asymmetrical behavior discussed in Section VII-A (see Fig. 13).

The stiffness of the two prototypes is computed as in (22) and (21) for the five interesting points visible in Fig. 13. These points show respectively: the point in which for null external load the stiffness is minimum (**1**) and maximum (**2**, due to the pretensioning); the point in which the two motor torques work

[7]Indeed, it is worth noting that the load torque is configuration dependent, i.e. $\tau_l = mgl\sin(q)$.

in the same direction to double the external load sustainable (**3**) and finally the two most interesting points in which, for external torque equal to the maximum torque of each motor ($\tau_l = \tau_p$), the torque is split equally among the two motor-units (for the FNL case) or only on the linear motor-unit (for the HL case) (**4**) and held by the nonlinear motor unit (for both the configurations) (**5**).

Results: The resulting torque/stiffness workspaces for the two prototypes are reported in Fig. 13. It is worth noting that, as previously observed in the identification results, there is asymmetry between the two motor-spring units of the FNL configuration. This causes the range of stiffness to be different depending on the sign of the external torque. Instead, for the HL workspace, this asymmetrical behavior is reduced, but contrary the maximum stiffness achievable is smaller due to the elastic elements used[8]. Focusing on the left-hand side region of the plot in Fig. 13, we can see that, compared to the original configuration, the proposed configuration (HL) allows to enlarge the torque/stiffness range, especially for external torque close to the maximum torque of each motor $\tau_p \simeq \tau_l$ and up to twice this value. Furthermore, by replacing the nonlinear motor unit with a linear one, the range of stiffness available at non-negligible external torque is increased. The linear motor-unit can be used to hold the whole amount of external load without compromise the stiffness range, which in turn can be spanned by exploiting the nonlinear unit. These results can be also verified from Fig. 14a and Fig. 14b by comparing the violet diamond-marked lines of both the figures, that represent the stiffness behavior at point **4** of Fig. 13 during the experiments. The evaluation of the stiffness for the other interesting points (**1, 2, 3, 5**) in Fig. 14a and Fig. 14b confirms the torque/stiffness characteristic shown in Fig.13.

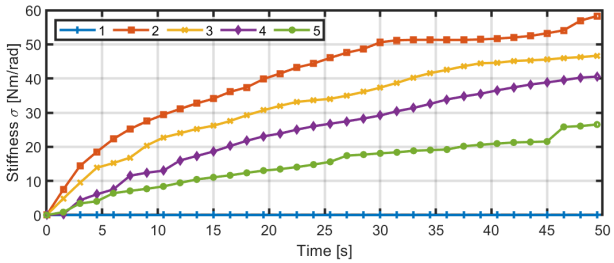

(a) FNL

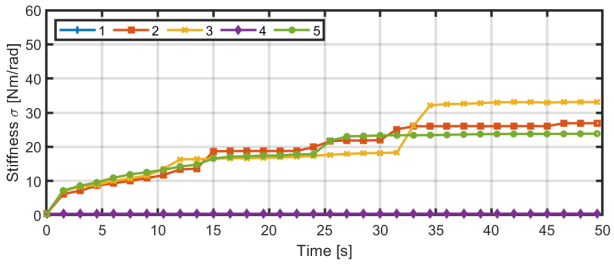

(b) HL

Fig. 14: Experimental results for the stiffness evaluation, using (22) and (21), of the two configurations. The five lines refer to the points in Fig. 13.

VIII. Discussion and Conclusion

The experimental results obtained in the previous section suggest that the models in (14) and in (19) well approximate the characteristics of the real prototypes proposed. Furthermore, the improvement in torque/stiffness performance brought by the proposed HL layout can be pointed out from the stiffness evaluation tests. Indeed, from Fig. 13 it is possible to conclude that the HL configuration allows us to carry higher external loads compared to the FNL configuration while maintaining the lower stiffness profile and the maximum variable stiffness range possible. This can be seen in Fig.14a and Fig. 14b by comparing the stiffness of the proposed layout with the benchmark one at point **4** (violet diamond-marked line). For the test-bed used, however, the variation range of the qbmove Advanced II prototype is smaller compared to the benchmark, but this can be easily overcome with the use of stronger springs. Indeed, by a suitable dimensioning of the elastic elements (linear and nonlinear), it is possible to adapt the minimum stiffness, and analogously the stiffness variation range, to the task requirements. This fact will be investigated in future works.

[8]The development of prototypes with higher stiffness capability is currently undergoing.

Besides this, experimental results showed that due to friction phenomena, all the characteristics present considerable torque and deflection biases and hysteresis cycles. Indeed, despite the nonlinear motor-spring units are theoretically symmetric, differences in the torque/deflection characteristics are visible. The cutting and pretensioning of the tendons are handmade and lead to different elongations that imply differences in final torques. Furthermore, the spring constants may have variable values from the nominal ones. Moreover, one minor limitation introduced by the HL configuration is due to the loss of symmetry of the mechanism. This particularity can be seen in the scheme in Fig. 1a. The loss of symmetry does not change the results presented in Fig. 13 and Fig. 14b for the low stiffness case (point/line **4**). Conversely, whenever we want to maintain high stiffness, but change the direction of the external load, the system has to pass through zero torque at the output shaft and, in turn, the output shaft position is altered. This implies that, differently from the benchmark prototype for which semi-sum and semi-difference of the motor positions can be used to control motion and stiffness [13], respectively, a different control scheme should be implemented for the qbmove Advanced II prototype. Future works intend to deal with this problem and to exploit different solutions for the placement of linear and nonlinear elastic elements.

In conclusion, the experimental results suggest that the proposed low-cost and modular VSA actuator, equipped with the novel HL configuration, can be particularly helpful for building high-performance compliant structures that preserve variable stiffness capability even in presence of high external loads, e.g. articulated and anthropomorphic robots with multiple degrees of complexity.

REFERENCES

[1] A. Albu-Schaffer, O. Eiberger, M. Grebenstein, S. Haddadin, C. Ott, T. Wimbock, S. Wolf, and G. Hirzinger, "Soft robotics," *IEEE Robotics & Automation Magazine*, vol. 15, no. 3, 2008.

[2] B. Vanderborght, A. Albu-Schäffer, A. Bicchi, E. Burdet, D. G. Caldwell, R. Carloni, M. Catalano, O. Eiberger, W. Friedl, G. Ganesh, *et al.*, "Variable impedance actuators: A review," *Robotics and autonomous systems*, vol. 61, no. 12, pp. 1601–1614, 2013.

[3] M. Garabini, C. Della Santina, M. Bianchi, M. Catalano, G. Grioli, and A. Bicchi, "Soft robots that mimic the neuromusculoskeletal system," in *Converging Clinical and Engineering Research on Neurorehabilitation II*, pp. 259–263, Springer, 2017.

[4] G. A. Pratt and M. M. Williamson, "Series elastic actuators," in *Intelligent Robots and Systems 95.'Human Robot Interaction and Cooperative Robots', Proceedings. 1995 IEEE/RSJ International Conference on*, vol. 1, pp. 399–406, IEEE, 1995.

[5] F. Negrello, M. Garabini, M. G. Catalano, J. Malzahn, D. G. Caldwell, A. Bicchi, and N. G. Tsagarakis, "A modular compliant actuator for emerging high performance and fall-resilient humanoids," in *Humanoid Robots (Humanoids), 2015 IEEE-RAS 15th International Conference on*, pp. 414–420, IEEE, 2015.

[6] N. G. Tsagarakis, M. Laffranchi, B. Vanderborght, and D. G. Caldwell, "A compact soft actuator unit for small scale human friendly robots," in *Robotics and Automation, 2009. ICRA'09. IEEE International Conference on*, pp. 4356–4362, IEEE, 2009.

[7] C. Knabe, R. Griffin, J. Burton, G. Cantor-Cooke, L. Dantanarayana, G. Day, O. Ebeling-Koning, E. Hahn, M. Hopkins, J. Neal, *et al.*, "Designing for compliance: Escher team valor's compliant biped," *Journal of field robotics*, 2016.

[8] M. Hutter, C. Gehring, D. Jud, A. Lauber, C. D. Bellicoso, V. Tsounis, J. Hwangbo, K. Bodie, P. Fankhauser, M. Bloesch, *et al.*, "Anymal-a highly mobile and dynamic quadrupedal robot," in *2016 IEEE/RSJ International Conference on Intelligent Robots and Systems (IROS)*, pp. 38–44, IEEE, 2016.

[9] A. Jafari, N. G. Tsagarakis, and D. G. Caldwell, "A novel intrinsically energy efficient actuator with adjustable stiffness (awas)," *IEEE/ASME transactions on mechatronics*, vol. 18, no. 1, pp. 355–365, 2013.

[10] N. G. Tsagarakis, I. Sardellitti, and D. G. Caldwell, "A new variable stiffness actuator (compact-vsa): Design and modelling," in *Intelligent Robots and Systems (IROS), 2011 IEEE/RSJ International Conference on*, pp. 378–383, IEEE, 2011.

[11] S. S. Groothuis, G. Rusticelli, A. Zucchelli, S. Stramigioli, and R. Carloni, "The vsaut-ii: A novel rotational variable stiffness actuator," in *2012 IEEE International Conference on Robotics and Automation*, pp. 3355–3360, IEEE, 2012.

[12] F. Petit, W. Friedl, H. Höppner, and M. Grebenstein, "Analysis and synthesis of the bidirectional antagonistic variable stiffness mechanism," *IEEE/ASME Transactions on Mechatronics*, vol. 20, no. 2, pp. 684–695, 2015.

[13] C. Della Santina, C. Piazza, G. M. Gasparri, M. Bonilla, M. G. Catalano, G. Grioli, M. Garabini, and A. Bicchi, "The quest for natural machine motion: An open platform to fast-prototyping articulated soft robots," *IEEE Robotics & Automation Magazine*, vol. 24, no. 1, pp. 48–56, 2017.

[14] E. C. Martinez-Villalpando and H. Herr, "Agonist-antagonist active knee prosthesis: a preliminary study in level-ground walking.," *Journal of Rehabilitation Research & Development*, vol. 46, no. 3, 2009.

[15] G. Tonietti, R. Schiavi, and A. Bicchi, "Design and control of a variable stiffness actuator for safe and fast physical human/robot interaction," in *Robotics and Automation, 2005. ICRA 2005. Proceedings of the 2005 IEEE International Conference on*, pp. 526–531, IEEE, 2005.

[16] M. Grebenstein, A. Albu-Schäffer, T. Bahls, M. Chalon, O. Eiberger, W. Friedl, R. Gruber, S. Haddadin, U. Hagn, R. Haslinger, *et al.*, "The dlr hand arm system," in *2011 IEEE International Conference on Robotics and Automation*, pp. 3175–3182, IEEE, 2011.

[17] M. G. Catalano, G. Grioli, M. Garabini, F. Bonomo, M. Mancini, N. Tsagarakis, and A. Bicchi, "Vsa-cubebot: A modular variable stiffness platform for multiple degrees of freedom robots," in *Robotics and Automation (ICRA), 2011 IEEE International Conference on*, pp. 5090–5095, IEEE, 2011.

[18] Y. Liu, X. Liu, Z. Yuan, and J. Liu, "Design and analysis of spring parallel variable stiffness actuator based on antagonistic principle," *Mechanism and Machine Theory*, vol. 140, pp. 44–58, 2019.

[19] P. Bilancia, G. Berselli, and G. Palli, "Virtual and physical prototyping of a beam-based variable stiffness actuator for safe human-machine interaction," *Robotics and Computer-Integrated Manufacturing*, vol. 65, p. 101886, 2020.

[20] W. Roozing, Z. Li, G. A. Medrano-Cerda, D. G. Caldwell, and N. G. Tsagarakis, "Development and control of a compliant asymmetric antagonistic actuator for energy efficient mobility," *IEEE/ASME transactions on mechatronics*, vol. 21, no. 2, pp. 1080–1091, 2015.

[21] R. Van Ham, T. G. Sugar, B. Vanderborght, K. W. Hollander, and D. Lefeber, "Compliant actuator designs," *IEEE Robotics & Automation Magazine*, vol. 16, no. 3, pp. 81–94, 2009.

[22] G. Grioli, S. Wolf, M. Garabini, M. Catalano, E. Burdet, D. Caldwell, R. Carloni, W. Friedl, M. Grebenstein, M. Laffranchi, *et al.*, "Variable stiffness actuators: The user's point of view," *The International Journal of Robotics Research*, vol. 34, no. 6, pp. 727–743, 2015.

[23] K. Melo, M. Garabini, G. Grioli, M. Catalano, L. Malagia, and A. Bicchi, "Open source vsa-cubebots for rapid soft robot prototyping," in *Robot Makers-Workshop in conjunction with 2014 Robotics Science and Systems Conference, Berkeley, California, USA*, 2014.

[24] J. Kirchhoff and O. von Stryk, "New insights in synthetic fiber rope elongation and its detection for ultra lightweight tendon driven series elastic robots," in *2017 IEEE International Conference on Advanced Intelligent Mechatronics (AIM)*, pp. 64–69, IEEE, 2017.

Riccardo Mengacci received a B.S. degree in Information and Automation Engineering from the Polytechnic University of Marche, Ancona in 2013 and a Master's Degree in Automation and Robotics Engineering from the University of Pisa in 2017. He is currently a Ph.D. student at the Research Center "E. Piaggio" of the University of Pisa and his research activity focuses on design and control strategies for robotics applications with a particular interest in compliant robots and impedance controlled robots.

Manolo Garabini graduated in Mechanical Engineering and received a Ph.D. degree in Robotics from the University of Pisa where he is employed as Assistant Professor. His main research interests are in the design, planning and control of soft and adaptive robots, from single joints, to complex multi-dof systems. He contributed to the realization of modular Variable Stiffness Actuators and in the design of the lower body of the humanoid robot WALK-MAN. He is the Principal Investigator in the THING EU Project for the University of Pisa.

Giorgio Grioli is a Researcher at the Italian Institute of Technology where he investigates design, modeling and control of soft robotic systems. He got his PhD in Robotics, Automation and Engineering from University of Pisa in 2011. He is author of more than 60 articles in the fields of soft robotic actuation, robot hand design and haptics. He serves as Associated Editor for ICRA and ICORR and is currently co-editing a special issue of the Actuators journal on "Variable Stiffness and Variable Impedance Actuators".

Manuel Catalano received a master degree in mechanical engineering and the doctoral degree in Robotics from the University of Pisa. He is currently a Researcher at the Italian Institute of Technology and a collaborator of the Research Center "E. Piaggio" of the University of Pisa. His main research interests are in the design of Soft Robotic systems, Human Robot Interaction and Prosthetic. In 2014, he won the Georges Giralt PhD Award, the prestigious annual European award given for the best PhD thesis by euRobotics AISBL.

Antonio Bicchi is Professor of Robotics at the University of Pisa, and Senior Scientist at the Italian Institute of Technology in Genoa. He graduated from the University of Bologna in 1988 and was a postdoc scholar at M.I.T. Artificial Intelligence lab in 1988/1990. He teaches Robotics and Control Systems in the Department of Information Engineering (DII) of the University of Pisa. He leads the Robotics Group at the Research Center "E. Piaggio" of the University of Pisa since 1990, where he was Director from 2003 to 2012. He is the head of the SoftRobotics Lab for Human Cooperation and Rehabilitation at IIT in Genoa. His main research interests are in Robotics, Haptics, and Control Systems